

# Structure, properties and rheological behavior of thermoplastic poly(lactic acid)/quaternary fulvic acid-intercalated saponite nanocomposites

Weijun Zhen<sup>1</sup> · Wentao Wang<sup>1</sup>

Received: 12 October 2014 / Revised: 13 September 2015 / Accepted: 30 September 2015 /  
Published online: 5 October 2015  
© Springer-Verlag Berlin Heidelberg 2015

**Abstract** Sodium humate was oxidized with nitric acid to obtain fulvic acid (FA), which was further quaternized to obtain quaternary fulvic acid (QFA). QFA-intercalated saponite (QFA-saponite) was prepared ultrasonically. Thermoplastic poly(lactic acid) (PLA)/quaternary fulvic acid-intercalated saponite nanocomposites were prepared by melt intercalation technique. The morphology and dispersion of QFA-saponite were investigated by X-ray diffraction, scanning electron microscopy, and transmission electron microscopy. Mechanical properties, thermal stability and crystallization behavior of PLA/QFA-saponite nanocomposites were also tested. Results showed a predominantly flocculated structure and partially intercalated morphology for QFA-saponite. Mechanical testing and thermogravimetric analysis showed that the tensile strength, impact properties, and thermostability of PLA/QFA-saponite nanocomposites improved significantly compared to pure PLA. Differential scanning calorimetry results showed that crystallinity of PLA increased from 22.5 to 68.3 % on addition of QFA-saponite. Polarized optical microscopy showed QFA-saponite as a nucleating agent for PLA that enhanced its crystallization rate. Rotational rheological behaviors of PLA/QFA-saponite nanocomposites demonstrated that incorporation of QFA-saponite increased rigidity of the network structure in PLA matrix.

**Keywords** Saponite · Fulvic acid · Poly(lactic acid) · Nanocomposites · Melt processing · Properties

---

✉ Weijun Zhen  
zhenweijun@xju.edu.cn

<sup>1</sup> Key Laboratory of Oil and Gas Fine Chemicals, Ministry of Education and Xinjiang Uygur Autonomous Region, Xinjiang University, Ürümqi 830046, China

## Introduction

The research and development of biodegradable polymers has attracted more and more attention, due to increased awareness of environmental issues [1, 2]. PLA, aliphatic thermoplastic polyester, is perhaps the most popular commercial biodegradable material, since it is not only biodegradable, but also compostable and nontoxic to the human body and to the environment. Moreover, PLA can be produced from renewable plant resources (starch and sugar) [3–5]. However, some of its physical properties, such as toughness, dimensional stability, melt viscosity, and crystallization rate are not satisfactory for processing and applications [6–10]. Therefore, there is a sustained interest in overcoming these limitations, without a major loss in its general performance, to meet the requirements in various end-use applications.

Over the past few years, PLA/layered silicate nanocomposites have been extensively studied, with an aim to improve the properties of PLA, such as, crystallinity, thermal and mechanical stabilities, gas permeability, degradation and flame retardancy [11, 12]. During the preparation of PLA/layered silicate nanocomposites, three main techniques are generally employed: in situ polymerization, solution intercalation, and melt intercalation. The melt intercalation method is considered to be the most useful method, especially for industrial processes, since melt methods are more simple, effective, and economical [13, 14].

Absence of interfacial interaction between the dispersed filler and polymer matrix often induces micro-phase separation for most conventional polymer-based nanocomposites [15, 16]. The nanofillers can be made compatible with the polymer bulk phase, by an organic treatment, which improves the thermal stability, stiffness and processability of PLA. Many academic institutions and industries have focused their researches to tackle the problems associated with filler aggregation [17–19].

Saponite is a kind of rare trioctahedral layered silicates. The hydrophilic nature of saponite limits its compatibility with organophilic polymers. However, chemical modification of saponite makes it compatible with the organophilic polymer, which is a key to the preparation of PLA/layered silicate nanocomposites.

Humic substances (HSs) are yellow and dark-brown colored naturally occurring organic compounds, widely found in peat and different types of coal, such as weathered coal and lignite. The origin, composition, and structure of HSs are very complicated to be specifically defined. Molecular weights of HSs generally vary from hundreds to millions [20, 21]. HSs contain a variety of functional groups, such as carboxyl, phenolic, alcoholic, ether, ketone, aldehyde, ester, amide, and others. Based on their solubilities in acidic and alkaline solutions, HSs can be divided into fulvic acid (FA; alkali soluble, acid soluble), humic acid (HA; alkali soluble, acid insoluble), and humin (alkali insoluble, acid insoluble). Compared to other HA, FA contains more number of oxygen-containing functional groups and is soluble at any pH. The structure and chemical compositions are determined by the source material and environment [22–24]. Moreover, FA has lower molecular weight, shows greater biological activity and finds applications in agriculture and industrial fields. In the recent years, many studies pointed out that FA forms a film on the mucus epithelium

of the gastrointestinal tract and protects it against infections and toxins. Therefore, FA has antimicrobial and anti-inflammatory properties [25–27].

In the present study, FA obtained from weathered coal was used. Due to presence of different functional groups and their numbers (mainly hydroxyl and the carboxyl) in its molecular structure, FA could easily react with ammonia to form amide and quaternary ammonium salt via amine methylation and quaternization reaction. The synthesized QFA served as an organo-modifier for the saponite and PLA/QFA-saponite nanocomposites in improving the comprehensive performance of PLA materials by melt intercalation. The structure, properties and rheological behavior of PLA/QFA-saponite nanocomposites and the effects of QFA-saponite on crystallization of PLA materials were studied.

## Experimental

### Materials

Sodium humate, prepared from weathered coal, was provided by Qitai Humate Plant in Xinjiang. Analytically pure nitric acid, methanal, ammonia solution, and dimethylamine were purchased from Kelong Chemical Co., China. PLA (L-form, injection grade,  $M_v = 80,000$  g/mol) was purchased from Shenzhen Guanghua-weiye Industrial Co., China. Acetyl tributyl citrate (ATBC) (industrial grade, plasticizer) was obtained from Changzhou Tianzheng Chemical Technology Co., China. Natural saponite powder, with an average grain size of approx. 60–70  $\mu\text{m}$  was purchased from Xinjiang Tuogema Colloid Co., China.

### Sample preparation

Preparation of FA: HA-Na was air-dried, crushed and sieved through a 75  $\mu\text{m}$  sieve. HA-Na was oxidized in a 2 mol/L  $\text{HNO}_3$  solution (concentration of the solution was 1 g per 10 mL) under mechanical stirring at 60 °C for 3 h. The extracted solution was separated from mixed solution by centrifugation at 4000 rpm for 5 min. This supernatant filtrate was filtered under vacuum, and then concentrated initially on a rotary evaporator at 55 °C under vacuum, and finally freeze-dried to obtain powdered FA.

Synthesis of QFA followed the scheme shown in Fig. 1. FA powder (10 g) and 20 mL aqueous ammonia solution [28 % (v/v)] were taken in a three-necked round-bottom flask and placed in an oil bath. The reaction was allowed to continue for 0.5 h during which, the ammonium salt dehydrated producing the FA amide. Subsequently, equal amount of methanal and FA amide were mixed together at pH 7–9, adjusted by adding 1 mol/L  $\text{Na}_2\text{CO}_3$  solution. After stirring for 1 h at 60–70 °C, dimethylamine was added and the solution stirred for further 3 h at 45 °C. Finally, the solution mixture was cooled and an equal amount benzyl chloride with the dimethylamine was added to it. The reaction was stirred for 3 h at 80 °C and freeze-dried to obtain QFA powder.

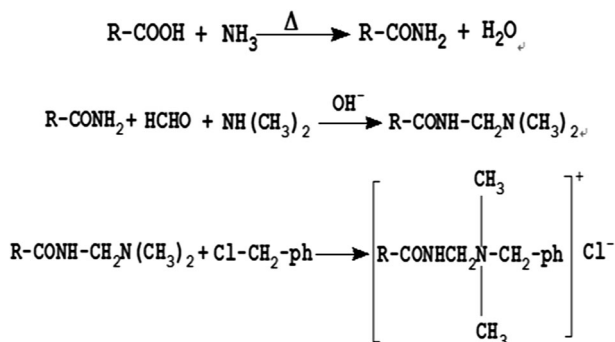


**Fig. 1** Reaction scheme for the synthesis of QFA

Preparation of QFA-saponite: QFA-saponite was prepared by a cation-exchange reaction of QFA. Saponite (1 g) was dispersed in 50 mL distilled water under mechanical stirring at 60 °C for 3 h. In a separate flask, QFA (1 g) was dissolved in 10 mL distilled water under mechanical stirring at 60 °C for 3 h. This QFA solution was then added dropwise into the saponite slurry. This reaction mixture was then sonicated in an ultrasonic cleaner (KQ5200B Kunshan Ultrasonic Instrument Co. Ltd.) at 60 °C for 8 h. The reaction mixture was filtered, followed by washing the precipitate with deionized water until no  $\text{Cl}^-$  (examined by 0.1 mol/L  $\text{AgNO}_3$ ) was detected and then dried to obtain QFA-saponite.

Preparation of PLA/QFA-saponite nanocomposites: PLA, ATBC and QFA-saponite were mixed in a high-speed mixer (1000 rpm) at room temperature for 20 min. The resultant mixture was sealed for 24 h to allow sufficient diffusion of plasticizers into PLA. The amount of PLA resin was 150 g. The amount of QFA-saponite added was expressed as parts per hundred of PLA resin (phr). The proportions of the reactants used for mixing are shown in Table 1. These mixtures were manually fed into the single screw extruder (HAAKE RHEOMEX 254, diameter 19 mm and L/D = 25:1, Germany) with a screw speed of 30 rpm, and the temperature profile along the extruder barrel was 170, 180, 180, and 180 °C (from feed zone to die). After these mixtures were extruded and pelletized, they were

**Table 1** Description of PLA/QFA-saponite nanocomposites

Sample designation	Composition		
	PLA (g)	QFA-saponite (g)	ATBC (g)
PLA	150	–	–
PLA0	150	–	15
PLA1	150	0.45	15
PLA2	150	0.75	15
PLA3	150	1.50	15
PLA4	150	4.50	15
PLA5	150	7.50	15

molded using the HAAKE MiniJet injection molding machine under a pressure of 80 MPa at 180 °C and pressure-holding time of 10 s.

## Characterization

The Fourier transform infrared (FTIR) spectra of the samples were recorded on a FTIR spectrophotometer (BRUKER-EQUINOX 55, Germany), using the standard KBr pellet disc technique. Spectra were recorded in the spectral range from 4000 to 400  $\text{cm}^{-1}$  at a resolution of 4  $\text{cm}^{-1}$ .

Raman spectra were recorded on a Bruker FT-Raman spectrometer VERTEX-70 (Bruker Optics, Germany) using diode pumped Nd:YAG lasers at an operating wavelength of 1064 nm. The measurements were performed using the 180° angle scattering geometry with 100 scans and a laser power of 500 mW at the sample location.

X-ray diffraction (XRD) patterns were recorded on a Philips X'Pert X-diffractometer (Netherlands), using  $\text{CuK}\alpha$  radiation at  $\lambda = 0.1540$  nm (50 kV, 35 mA). Diffraction spectra were obtained over  $2\theta$  range of 1.5°–60° with a scanning speed of 0.1°/s. Powdered saponite and QFA-saponite samples were used for this analysis.

Differential scanning calorimetry (DSC) was carried out using a NETZSH 204 DSC differential scanning calorimeter (Germany). Samples of about 6 mg each were used for the analysis and heated from room temperature to 200 °C at a heating rate of 10 °C/min under a nitrogen flow.

Thermal gravimetric analysis (TGA) was conducted on TA-2000 analyzer (USA). The samples were dried in a vacuum oven at 60 °C for 24 h before testing. Samples of about 5 mg to be tested were placed in an open alumina crucible. The analysis was carried out at a heating rate of 10 °C/min from 30 to 600 °C. All the measurements were carried out with a nitrogen flow rate of 100 mL/min.

The morphologies of the QFA-saponite and impact fracture surfaces of PLA/QFA-saponite nanocomposites were observed by a scanning electron microscope (SEM, Inspect F, FEI Instrument Co. Ltd., Netherlands) at an accelerated voltage of 20 kV. Prior to SEM evaluation, the samples were sputter-coated with gold to avoid electrical charging during the tests.

The morphologies of saponite and QFA-saponite were also observed by transmission electron microscope (TEM), using TECNAI G2 F20 (FEI Co., Netherlands). Saponite or QFA-saponite was mixed with ethanol and sonicated for 30 min. Then 2–3 drops of each homogeneous mixture was coated on the micro-grid using glass capillary. After most of the ethanol vaporized gradually, the sample was observed by the transmission electron microscope at an accelerated voltage of 200 kV.

The morphologies of PLA/QFA-saponite nanocomposites were also observed by the transmission electron microscope (TEM), TECNAI G2 F20 (FEI Co., Netherlands). The ultracryotomy of PLA/QFA-saponite nanocomposite samples was done using LEICA EM UC6/F6 microtome. The thickness of ultracryotomy was about 80 nm. Specimens were tested at an accelerated voltage of 200 kV.

Crystallization was studied by polarized optical microscopy (POM) (LEICA-DMLP1, Germany). The sample was melted at 200 °C for 3 min and then rapidly

cooled to a preset temperature for isothermal crystallization. PLA spherulites were observed in the micrographs after isothermal crystallization.

The samples were tested for tensile strength according to ASTM D412-80, using an Instron 4302 Universal Testing Machine (USA) at a crosshead speed of 5 mm/min. A minimum of five measurements for each sample were recorded. Samples of PLA/QFA-saponite nanocomposites were dried in a vacuum oven at 60 °C for 24 h before testing.

Notched izod impact testing was carried out using a Testing Machines Inc. 43-02-01 Monitor/Impact machine according to ASTM D256. 2-mm-deep notches were cut into sample beams using a TMI notch cutter. All results presented were the average values of five measurements.

The rotational rheological measurement was carried out on a rotational rheometer (Gemini 200 rheometer, Bohlin Co., UK) equipped with a parallel plate, 25 mm in diameter at 170 °C and frequency range from 0.1 to 100 rad/s. Storage moduli ( $G'$ ), and complex viscosities ( $\eta^*$ ) were measured in the frequency sweep mode.

## Results and discussion

### Characterization

#### *FTIR spectra analysis*

Figure 2 shows the FTIR spectra in the region 4000–500  $\text{cm}^{-1}$  for HA-Na, FA, and QFA. These spectra were compared to each other in order to determine the changes, such as, emergence of new peaks, variations in intensities of peaks originally present, and shifted in wavelengths. The spectra of HA-Na, FA, and QFA showed similar peaks. However, the relative intensities of some bands differed. The strong C=O stretching vibration around 1373  $\text{cm}^{-1}$  became more intense due to oxidization,

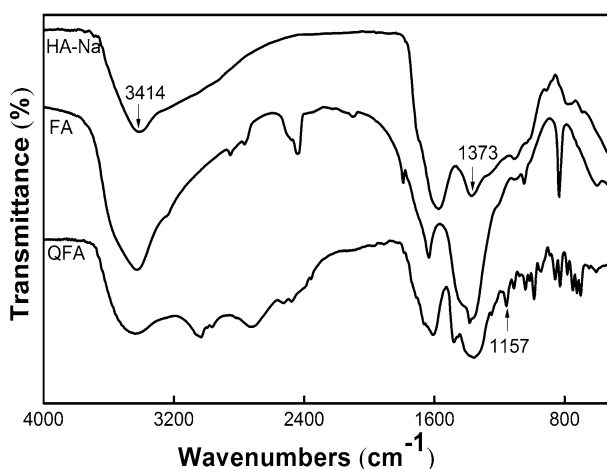


**Fig. 2** FTIR spectra of HA-Na, FA and QFA

suggesting that  $\text{COO}^-$  group of FA was affected due to oxidation. The most significant change in the FTIR spectra observed was the characteristic peak of C–N deformation at  $1157\text{ cm}^{-1}$ , which was due to the characteristic functional group of the desired QFA. The results suggested that QFA was synthesized under the given experimental conditions.

### FT-Raman analysis

The FT-Raman spectra of FA and QFA are shown in Fig. 3. Characteristic bands around  $3200\text{ cm}^{-1}$ , due to symmetric and asymmetric stretching vibrations of aliphatic C–H bonds in  $\text{CH}_3$  and  $\text{CH}_2$  groups, appeared in the spectrum. The Raman spectrum showed characteristic peaks for ammonium deformation at  $1040$  and  $622\text{ cm}^{-1}$ . It could be seen that the peaks that appeared in QFA were due to the formation of quaternary ammonium groups. The results of FT-Raman spectral analysis were consistent with the FTIR analysis.

### XRD analysis

X-ray diffraction patterns of saponite and QFA-saponite are shown in Fig. 4. Saponite showed several reflections in the  $2\theta$  range of  $2^\circ$ – $60^\circ$ , which indicated the presence of various hydrated monovalent and divalent cations, in the interlayer. Saponite yielded characteristics diffraction peaks at  $2\theta = 6.23^\circ$  (Fig. 4), which corresponded to the basal spacing  $d_{001}$  (1.407 nm). Saponite ions were exchanged with alkylammonium cations (QFA) during the preparation of organosaponite, and this exchange resulted in an increase in the d-spacing of the saponite interlayer. The XRD pattern of QFA-saponite (Fig. 4) also showed a strong and sharp diffraction band and the basal space of QFA-saponite was 1.566 nm ( $2\theta = 5.63^\circ$ ), which was significantly larger than that of saponite. The above increments in d-spacing suggested that the alkylammonium cations had intercalated into the saponite layers. The difference in d-spacing between the saponite and QFA-saponite was 0.159 nm.

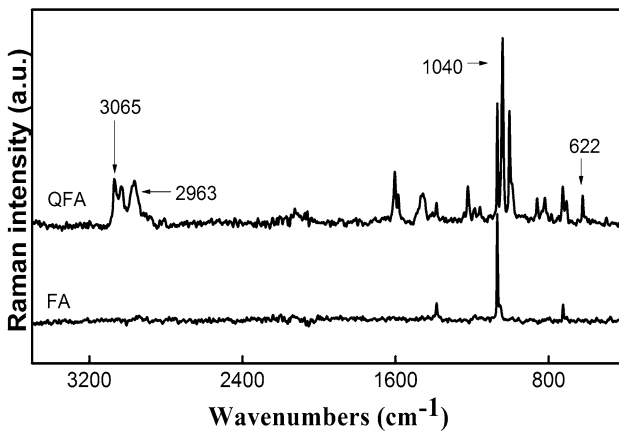
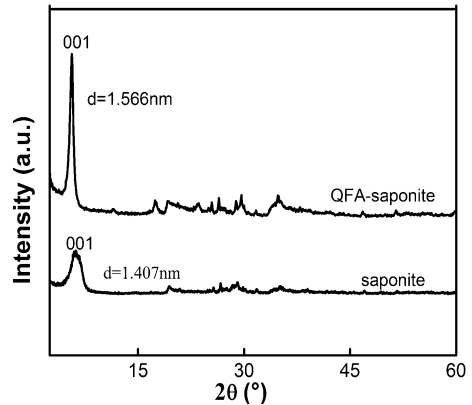


**Fig. 3** FT-Raman spectra of FA and QFA

**Fig. 4** XRD patterns of saponite and QFA-saponite



The presence of the shoulder ( $2\theta = 4.49^\circ\text{--}6.86^\circ$ ) in the diffraction pattern of QFA-saponite indicated a heterogeneous structure in the interlayer of saponite, which resulted in different surface charge densities of the saponite layers [28]. These diffraction patterns proved that the samples were polyphasic systems, composed of crystallites, containing saponite layers with various arrangements of the organic species (bilayer and paraffin-monolayer) and random interstratifications of such layers. The increased basal spacing of 0.159 nm upon the intercalation by QFA ammonium ions was compatible with the conformation of the lateral bilayer. The appearance of a shoulder at a lower  $2\theta$  angle may be attributed to the inclined paraffin-monolayer structure, with the ammonium groups in direct contact with the silicate layer and the long alkyl chains having a maximum angle of  $90^\circ$  [29].

Figure 5 shows the XRD patterns of QFA-saponite and PLA/QFA-saponite nanocomposites. The QFA-saponite sample showed a single diffraction peak at

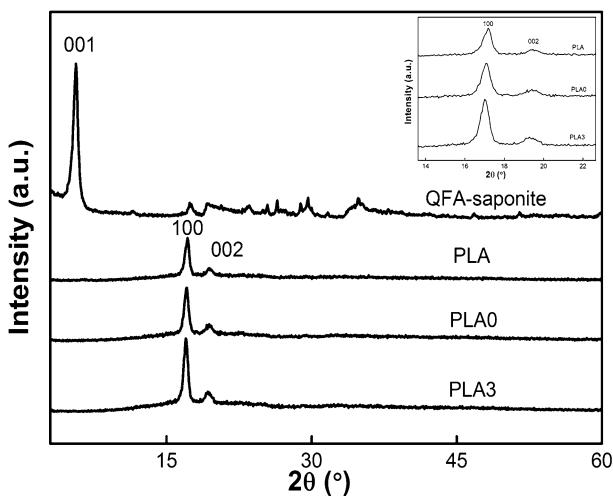


**Fig. 5** XRD patterns of QFA-saponite and PLA/QFA-saponite nanocomposites



$2\theta = 5.64^\circ$ , corresponding to the basal reflection of (001) plane, accounting for an interlayer spacing of 1.566 nm as shown in Fig. 4. As expected, the crystalline PLA exhibited a very strong reflection peak at  $2\theta = 17.1^\circ$  due to diffraction from (100) and another reflection peak at  $2\theta = 19.5^\circ$  from the (002) plane [30]. After the introduction of QFA-saponite into PLA, the most significant features of PLA3 were found in the lower angle range, which explained the structure of the QFA-saponite. For the PLA3, diffraction peak at low angle region could not be distinguished, probably due to the exfoliation of the QFA-saponite, which was also evident from the TEM analysis (Fig. 8). This indicated an achievement of further exfoliation of saponite by PLA after the melt-blending. The further elucidation of the saponite structure was carried out by TEM analysis.

### Morphological investigation

Scanning electron microscopy micrographs of saponite and QFA-saponite are shown in Fig. 6. The unmodified saponite showed a uniformly layered structure. The surface of the saponite was leveled and smoothed (Fig. 6a). QFA-saponite showed significant morphological changes, after exchange of ions with QFA, as clearly seen in the figure (Fig. 6b). After addition of QFA, the surface of the QFA-saponite became relatively folded and disordered, and therefore, more expansion between layers was expected. However, small and aggregated particles were observed on the surface of QFA-saponite.

The fracture characteristics of PLA were obtained from SEM images. Figure 7 shows the SEM images of tensile fractured surfaces of neat PLA, PLA0 and PLA3. Neat PLA showed a relatively smoother and complete fractured surface, indicative of a brittle fracture. However, the surface roughness of fractured area of PLA0 was clearly increased compared to the neat PLA. And some tiny filaments were adhered to the rough phase interface of PLA0, which was the characteristic of toughness fracture. This was due to the effect of ATBC, since ATBC was added as a plasticizer to increase the flexibility of the PLA macromolecules, extend the relaxation process of PLA, and improve the toughness of PLA. The similar result was also reported by Tsou et al. [31]. Furthermore, PLA3 showed a much rougher phase interface with numerous filaments and toughness cavities, which proved to be a typical toughness fracture and explained the improvement in toughness on the introduction of QFA-saponite.

TEM morphologies of saponite and PLA3 are shown in the Fig. 8. In Fig. 8a, the dark region represented the saponite phase, in which the saponite layers appear aggregated together. In Fig. 8b, the flocculated structure and partially intercalated morphology of saponite can be clearly observed, and the d-spacing between the layers of saponite appear enlarged. The TEM morphological analysis supported the XRD results. This indicated that QFA-saponite with a strong polarity intercalated easily into the PLA matrix and further enlarged the space between the interlayers. This could be explained on the basis that saponite is a multilayer silicate mineral, having galleries that naturally contain inorganic cations, which balance the charges of the oxide layers, in a hydrophilic environment [32–34]. Meanwhile, QFA-saponite also provided functional groups that could react or interact with the

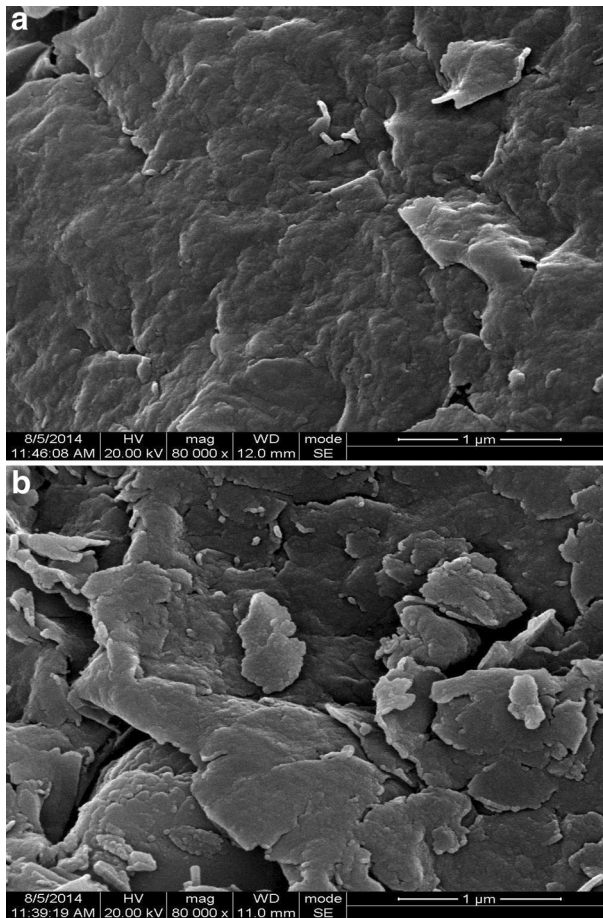


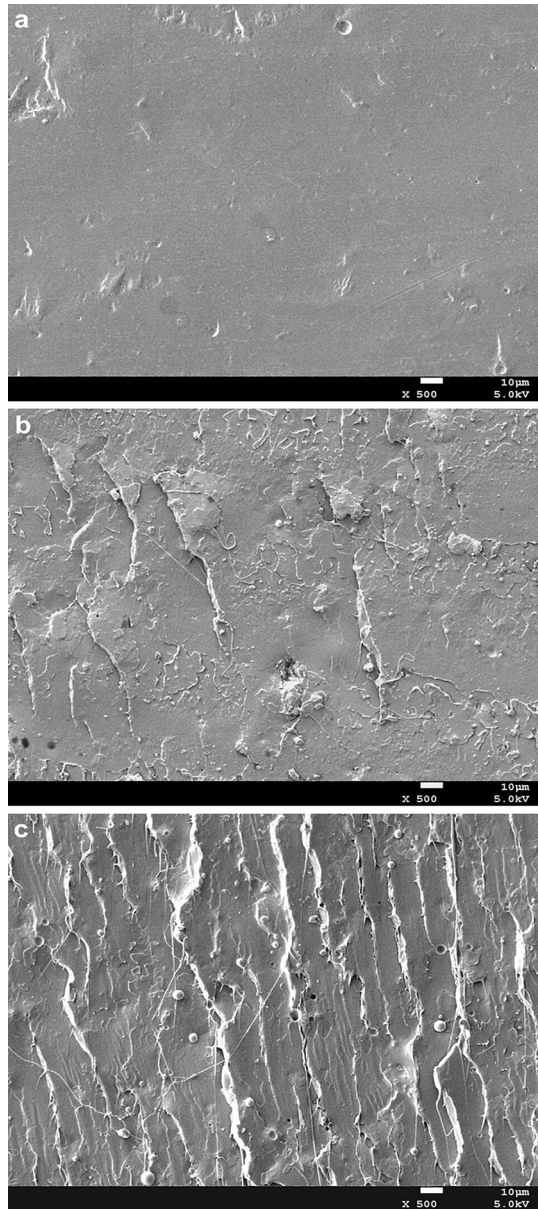
**Fig. 6** SEM images of saponite and QFA-saponite (**a** saponite, **b** QFA-saponite)

monomer or polymer that improved the interfacial strength between the saponite and polymer matrix. In conclusion, better mechanical properties were achieved for PLA/QFA-saponite nanocomposites, which were also proved by mechanical tests.

#### *TGA-DTG analysis*

Thermal stabilities of pristine PLA and its nanocomposites were tested by thermogravimetric analysis (TGA) under nitrogen gas atmosphere as shown in Fig. 9. All specimens displayed two degradation steps, when heated from room temperature to 600 °C at a ramp rate of 10 °C/min. In order to study the degradation thoroughly, the initiation temperature ( $T_{\text{onset}}$ ), maximum temperature ( $T_{\text{max}}$ ), final decomposition temperature ( $T_{\text{end}}$ ) and residues obtained at 500 °C ( $r_{500\text{ °C}}$ ) are presented in Table 2.

**Fig. 7** SEM images of fracture surface of PLA, PLA0 and PLA3 (**a** PLA, **b** PLA0, **c** PLA3)



The values for  $T_{\text{onset}}$  and  $T_{\text{max}}$  of PLA3, summarized in Table 2, were higher than those of neat PLA. In particular,  $T_{\text{max}}$  of PLA was enhanced by about 10 °C. The  $T_{\text{end}}$  and  $r_{500\text{ °C}}$  increased on addition of QFA-saponite that confirmed the compatibility of QFA-saponite with PLA matrix. The introduction of the QFA-saponite layers greatly improved the thermal properties of the polymer matrix. The results showed that the degradation rates of the nanocomposites reduced

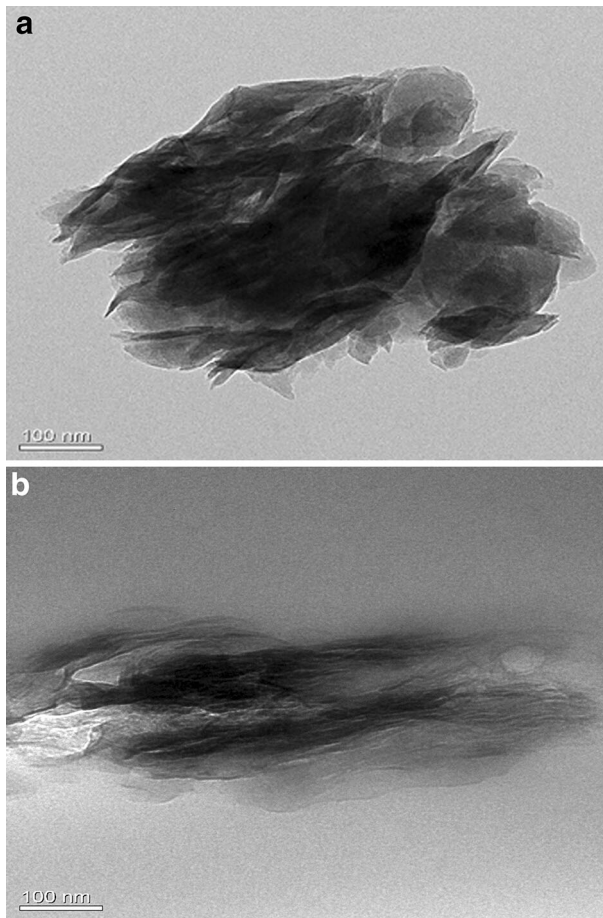


**Fig. 8** TEM images of saponite and PLA3 (**a** saponite, **b** PLA3)

significantly compared to that of PLA, which indicated an improvement in thermal stability of PLA. This could be attributed to the prevention of quick expansion of heat, due to the inorganic material that limits further degradation. The effects of thermal stabilization of nanoclay could be explained by the so-called Labyrinth barrier effect, caused due to the dispersion of the highly anisotropic layered silicate platelets, on the nanometer scale, in PLA, which hindered the diffusion of the volatile degradation products (carbon dioxide, carbon monoxide, water molecules, etc.) from the bulk of the polymer matrix to the gaseous phase [35, 36].

#### *DSC analysis*

Figure 10 presents the DSC thermograms of PLA, PLA0 and PLA3, respectively. The DSC thermal parameters of PLA, PLA0 and PLA3 are summarized in Table 3.

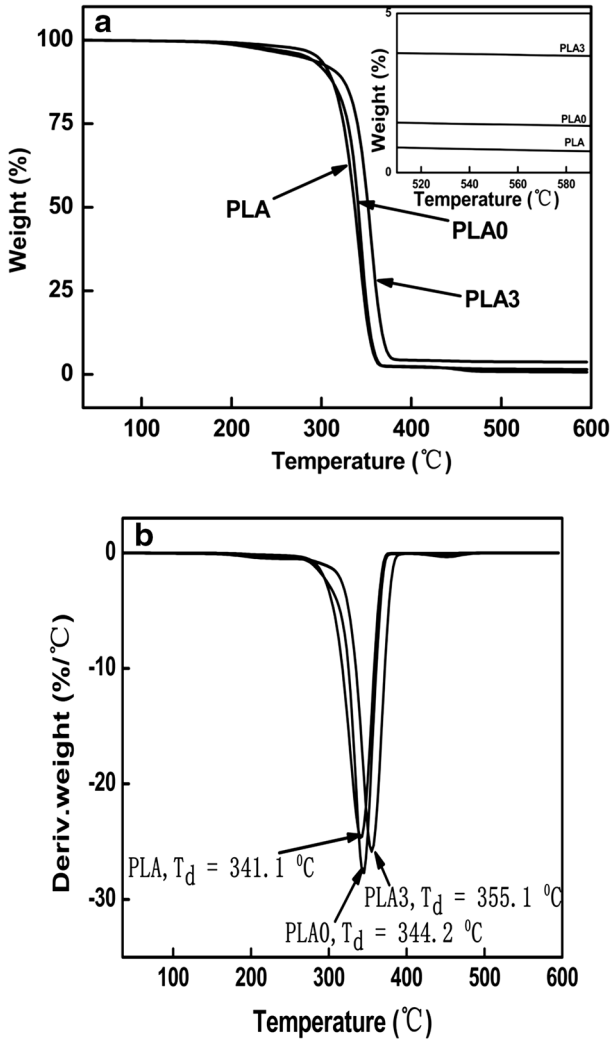


**Fig. 9** TGA-DTG curves of PLA, PLA0 and PLA3 (a TG, b DTG)

**Table 2** The thermogravimetric analysis (TGA) results of PLA, PLA0 and PLA3 nanocomposites

Sample	$T_{onset}$ (°C)	$T_{max}$ (°C)	$T_{end}$ (°C)	$r_{500\text{ }^\circ\text{C}}$ (wt%)
PLA	312.4	341.1	357.3	0.7
PLA0	315.3	344.2	357.9	1.5
PLA3	328.2	355.1	370.6	3.7

**Fig. 10** DSC thermograms of PLA, PLA0 and PLA3

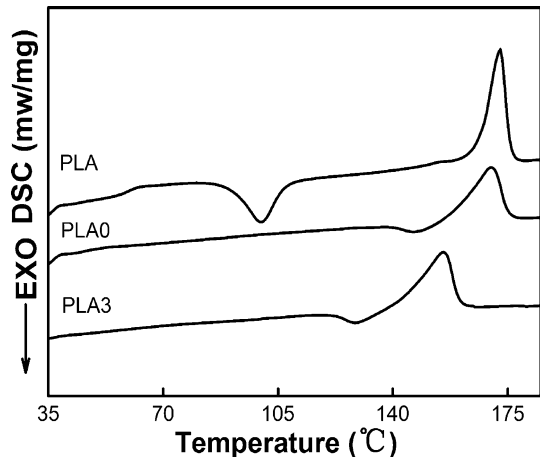


**Table 3** Thermal characteristics of PLA, PLA0 and PLA3

Sample	$T_c$ (°C)	$T_m$ (°C)	$\Delta H_c$ (J/g)	$\Delta H_m$ (J/g)	$X_c$ (%)
PLA	99.7	172.7	29.4	50.3	22.5
PLA0	–	170.5	–	45.7	54.1
PLA3	–	155.3	–	57.2	68.3

The degree of crystallinity ( $X_c$ ) was determined from DSC analysis data according to Eq. (1), where  $\Delta H_m$ ,  $\Delta H_c$  and  $\Phi_{\text{PLA}}$  are the measured melting enthalpy, cold-crystallization enthalpy, and weight fraction of PLA, respectively. In Table 3,  $T_m$  and  $T_c$  are the measured melting temperature and cold-crystallization temperature, respectively.

$$X_c = \frac{\Delta H_m - \Delta H_c}{\phi_{\text{PLA}} \Delta H_m^0} \times 100 \% \quad (1)$$

An enthalpy of fusion ( $\Delta H_m^0$ ) of 93.6 J/g, was used for the perfectly crystalline PLA phase [37].

Table 3 shows that  $T_m$  of PLA was 172.7 °C, whereas  $T_m$  of PLA0 decreased to 170.5 °C, due to plasticization of PLA by ATBC. Furthermore,  $T_m$  of PLA3, loaded with QFA-saponite, significantly decreased to 155.3 °C, which demonstrated that QFA-saponite also had a synergistic plasticization effect, since QFA-saponite could generate hydrogen bonding with PLA and broke the intermolecular interactions in PLA. Moreover, Fig. 10 shows that  $\Delta H_m$  of PLA3 increased by 13.7 % compared to that of PLA. Figure 10 also shows that the cold crystallization peak of PLA disappeared after introduction ATBC during processing by the melt intercalation method. Additionally, ATBC also enhanced the crystallization rate of PLA. Consequently,  $X_c$  of PLA increased from 22.5 to 54.1 %. On the other hand,  $X_c$  of PLA3 increased from 54.0 to 68.3 %, which indicated that the crystallinity of the

PLA clearly increased due to the heterogeneous nucleation of the QFA-saponite [38].

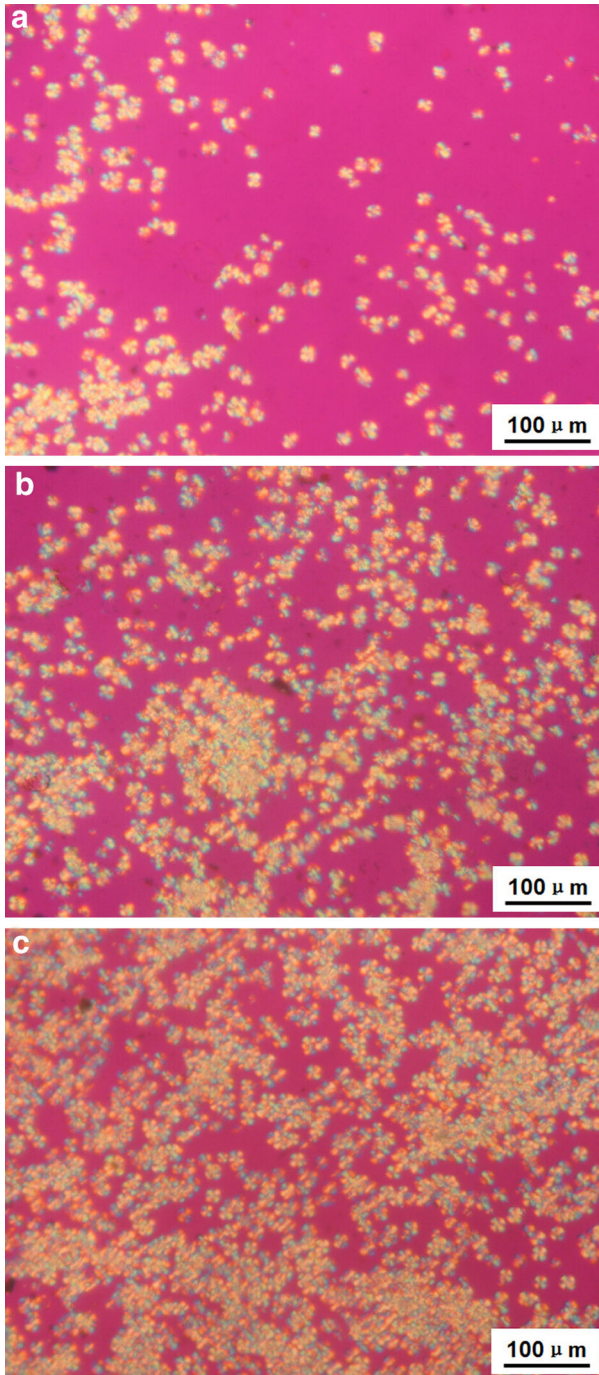
### *POM analysis*

Figure 11 shows POM images of PLA, PLA0, and PLA 3, crystallized isothermally at 130 °C for 15 min. As seen in Fig. 11, the spherulites of PLA grew bigger and collided with each other, resulting in diameters reaching 50–100  $\mu\text{m}$ . The sizes of the PLA0 spherulites were reduced to 5–10  $\mu\text{m}$  or less, with a non-uniform distribution. As for PLA3, very fine crystals with blurred boundaries were observed and the nucleation densities were increased with the introduction of QFA-saponite. On comparing the crystalline morphologies of the three PLA samples, it was apparent that QFA-saponite provided the largest number of nuclei that accelerated the crystallization rate. POM analysis further confirmed that QFA-saponite induced the crystallization of PLA more efficiently, which was in accordance with the aforementioned DSC results.

It is well known that two main mechanisms, namely chemical nucleation and epitaxial nucleation, have been widely accepted to elucidate the nature of nucleation process, on addition of nucleating agents in polymers [39]. As regards the chemical nucleation, the nucleating agent dissolves in the polymer melt and reacts with it, leading to the scission of polymer chains and the formation of ionic end groups, which constitute a true nucleating species [40]. In the present work, PLA was not able to react with ATBC or QFA-saponite, which indicated that chain scission of PLA was not a result of the chemical reaction, occurring during the melting process. Consequently, the possibility of a nucleation mechanism of PLA induced by the chemical reaction between PLA, ATBC, and QFA-saponite was ruled out. With regard to epitaxial nucleation, the polymer chains epitaxially grow on the surface of nucleating agent, through a physical interaction, where a good lattice matches the two crystalline structures of polymer and nucleating agent. With regard to the present work, the hydrogen bonding interactions between PLA and QFA-saponite probably play an important role in the nucleation process. However, additional information is still needed for an in-depth investigation of the exact nucleation mechanism.

### **Testing of mechanical properties**

Table 4 shows the mechanical properties of PLA/QFA-saponite nanocomposites. It was evident from Table 4 that maximum tensile strength was achieved with the addition of 1 phr QFA-saponite to PLA. This suggested that QFA-saponite acted as reinforcing filler, which increased interaction at the boundaries of the phases, upon the addition of 1 phr QFA-saponite. Strong interphase interaction between the matrix and the dispersed phase was believed to reduce the stress concentration point, when tensile load was applied. The QFA-saponite was able to act as reinforcing filler, due to its high aspect ratio and platelet structure. However, when the amount of QFA-saponite was more than 1 phr, only a part of QFA-saponite localized in the interfacial area, and the excess was dispersed in the matrix, which



**Fig. 11** POM images of PLA, PLA0, and PLA3 crystallized isothermally at 130 °C for 15 min (**a** PLA, **b** PLA0, **c** PLA3)



**Table 4** Mechanical properties of PLA/QFA-saponite nanocomposites

Sample	Maximum tensile strength (MPa)	Elongation at break (%)	Impact strength (J/cm <sup>2</sup> )
PLA	40.65 ± 2.6	5.89 ± 0.4	2.98 ± 0.2
PLA0	46.65 ± 1.3	6.35 ± 0.8	3.14 ± 0.4
PLA1	47.43 ± 2.1	8.96 ± 0.5	3.43 ± 0.2
PLA2	48.34 ± 1.2	9.37 ± 0.7	3.67 ± 0.6
PLA3	50.02 ± 1.8	13.42 ± 0.5	5.37 ± 0.5
PLA4	43.13 ± 2.5	9.08 ± 0.9	4.47 ± 0.9
PLA5	30.75 ± 2.0	8.58 ± 1.0	3.65 ± 0.7

affected the homogeneity and the tensile strength of the blends [41]. Some of QFA-saponite was presented in the form of tactoids, partially intercalated and stacked which weakened the reinforcing effect, owing to poor dispersion of QFA-saponite and hence was unable to transfer the stress efficiently [42].

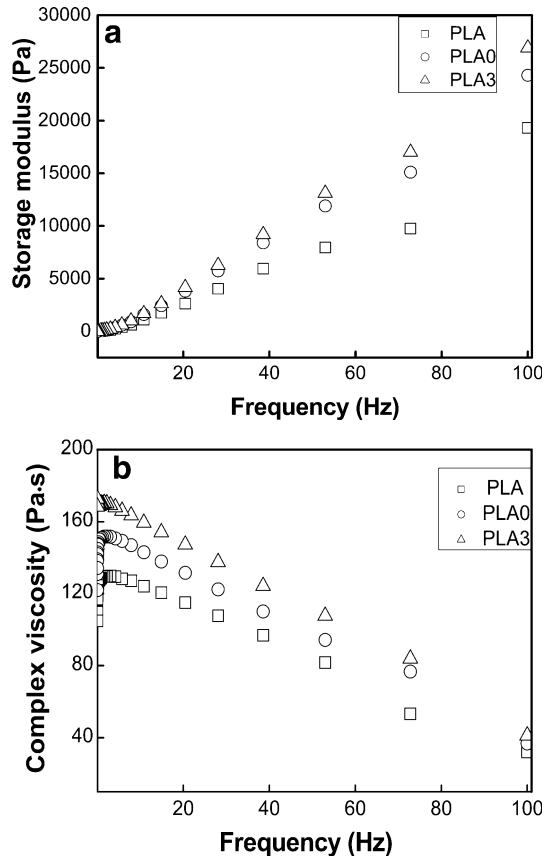
Table 4 also shows that the elongation at break for PLA/QFA-saponite nanocomposites reached a maximum at the 1 phr QFA-saponite, and then decreased with further increase in the amount of QFA-saponite. The peak value of elongation at break was 13.4 %, which was increased by 7.5 % compared to that of PLA. These results demonstrated that QFA-saponite was able to effectively restrain the crack propagation. At the same time, relative slip of QFA-saponite sheets also absorbed fractured energies, and improved elongation at break of PLA/QFA-saponite nanocomposites. When the content of QFA-saponite was more than 1 phr, some QFA-saponite particles aggregated due to interactions between the QFA-saponite layers, which reduced the interaction between PLA resin matrix and QFA-saponite that resulted in decreasing of elongation at break of PLA/QFA-saponite nanocomposites.

Table 4 also shows the notched impact strengths for the PLA, PLA0, and PLA3. As expected, the impact strength of PLA3 increased significantly on addition of QFA-saponite. The toughening effect further increased with increase in amount of QFA-saponite. The enhancement in impact strength of PLA/QFA-saponite nanocomposites could be due to the homogeneous dispersion and distribution of small domains of QFA-saponite in the PLA matrix [43, 44]. The QFA-saponite absorbed the impact strength and helped in concentration of stress during the impact deformation. The QFA-saponite component could induce energy dissipation mechanisms in PLA, which retarded the initiation and propagation of the crack that subsequently led to an improvement in toughness.

### Rheological analysis

The variations in storage moduli ( $G'$ ) and complex viscosities ( $\eta^*$ ) of PLA, PLA0, and PLA3, are depicted in Fig. 12. As seen in Fig. 12a, PLA3 exhibited an increase in the  $G'$  in the frequency range, investigated experimentally. This indicated slow transition of characteristics from the classical liquid state to the pseudosolid nature. Higher  $G'$  for PLA3 compared to that of the PLA matrix revealed the reinforcing

**Fig. 12** Rheological behavior of PLA, PLA0 and PLA3 (a storage modulus, b complex viscosity)



effect of QFA-saponite. This behavior was primarily the result of increase in rigidity of the network structure in the PLA matrix on incorporation of QFA-saponite.

Due to the nucleating effect of the intercalated/exfoliated QFA-saponite, the crystalline domain of the PLA showed good improvement. Similar facts of increased stiffness have been corroborated with the increased rheological properties of PLA3. Ray and coworkers [45] described similar behavior of increase in melt state rheological properties of polyester nanocomposites. They found that like other properties, rheological properties of nanocomposites were also directly related to the degree of dispersion of the silicate layers in the polymer matrix and level of interfacial interactions between the layered silicate surface and polymer chains.

The variations in complex viscosities ( $\eta^*$ ) as a function of frequency for PLA and PLA3 are depicted in Fig. 12b. It is evident that both, PLA and the PLA3, exhibited transitions to non-Newtonian pseudoplastic behaviors, within the deformation region of 0.01 to 100 Hz. As seen in the figures, the viscosities decreased consistently with increase in frequency, thus revealing typical characteristics of a completely frequency-dependent nature. PLA and PLA3 exhibited a shear thinning effect unlike other thermoplastic matrices. But the effect was more pronounced in

the case of PLA3 as compared with that of PLA. According to Pluta et al. [46], the real part of the complex viscosity is an energy dissipation term, similar to the imaginary part of the complex modulus.

The magnitude of  $\eta^*$  in case of PLA matrix was observed to be in the range of 10 to 7 Pa s, which increased considerably in PLA3 from 20 to 7 Pa s. This increase in the  $\eta^*$  over the entire experimentally investigated frequency region reflects the reinforcement effect of QFA-saponite within the molten PLA matrix. Iannace and Nicolais [47] attributed such an improvement in  $\eta^*$  for PLA3 compared to virgin PLA matrix to the reinforcing effect from the interaction between the PLA matrix and hydroxylated organic “surfactant” ends of QFA-saponite. Ray and Okamoto [48] attributed this behavior to the presence of stacks of intercalated/exfoliated silicate layers that are randomly oriented in the polymer matrix, forming a 3D network structure. These intercalated/exfoliated layers have only translational motion. A large-amplitude oscillatory shear is able to orient these structures, thereby increasing the coefficient of viscosity. Another explanation for such kind of behavior of improved  $\eta^*$  is probably due to the phenomenon of physical jamming of the dispersed saponite layers, owing to their highly anisotropic nature [49].

## Conclusions

Fulvic acid was prepared from HA-Na and nitric acid, which was then quaternized to QFA. QFA-saponite was prepared by ultrasonic intercalation. A series of novel PLA/QFA-saponite nanocomposites were prepared by melt intercalation method. A flocculated structure and partially intercalated morphology of PLA/QFA-saponite nanocomposites was confirmed by TEM. The intercalated saponite acted as a heterogeneous nucleating agent and accelerated the crystallization rate of PLA. Mechanical properties and thermostabilities of PLA/QFA-saponite nanocomposites were significantly improved with the addition of QFA-saponite. Rheological behaviors revealed the reinforcing and toughness effect of QFA-saponite.

**Acknowledgments** We greatly appreciate that this work is financially supported by National Science Foundation of China (51163013).

## References

1. Yu L, Dean K, Li L (2006) Polymer blends and composites from renewable resources. *Prog Polyme Sci* 6:576–602
2. Wang L, Cheng S, Zhuo R (2014) Syntheses and properties of novel copolymers of polycaprolactone and aliphatic polycarbonate based on ketal-protected dihydroxyacetone. *Polym Bull* 1:47–56
3. Dadbin S, Naimian F, Akhavan A (2011) Poly (lactic acid)/layered silicate nanocomposite films: morphology, mechanical properties, and effects of  $\gamma$ -radiation. *J Appl Polym Sci* 1:142–149
4. Peregó G, Cella GD, Bastioli C (1996) Effect of molecular weight and crystallinity on poly (lactic acid) mechanical properties. *J Appl Polym Sci* 1:37–43
5. Gattin R, Copinet A, Bertrand C, Couturier Y (2003) Biodegradation study of a coextruded starch and poly (lactic acid) material in various media. *J Appl Polym Sci* 3:825–831
6. Ali F, Chang YW, Kang SC, Yoon Yong J (2009) Thermal, mechanical and rheological properties of poly (lactic acid)/epoxidized soybean oil blends. *Polym Bull* 1:91–98

7. Harris AM, Lee EC (2008) Improving mechanical performance of injection molded PLA by controlling crystallinity. *J Appl Polym Sci* 107:2246–2255
8. Yuan Y, Ruckenstein E (1998) Polyurethane toughened polylactide. *Polym Bull* 4–5:485–490
9. Picard E, Espuche E, Fulchiron R (2011) Effect of an organo-modified montmorillonite on PLA crystallization and gas barrier properties. *Appl Clay Sci* 1:58–65
10. Su ZZ, Guo WH, Liu YJ, Li QY, Wu CF (2009) Non-isothermal crystallization kinetics of poly (lactic acid)/modified carbon black composite. *Polym Bull* 5:629–642
11. Nunez K, Rosales C, Perera R, Villarreal N, Pastor JM (2011) Nanocomposites of PLA/PP blends based on sepiolite. *Polym Bull* 9:1991–2016
12. Ahmadi SJ, Huang YD, Li W (2004) Synthetic routes, properties and future applications of polymer-layered silicate nanocomposites. *J Mater Sci* 39:1919–1925
13. Shen Z, Simon GP, Cheng YB (2002) Comparison of solution intercalation and melt intercalation of polymer–clay nanocomposites. *Polymer* 15:4251–4260
14. Pandey JK, Raghunatha Reddy K, Pratheep Kumar A, Sinch RP (2005) An overview on the degradability of polymer nanocomposites. *Polym Degrad Stabil* 2:234–250
15. Su XF, Zhang G, Xu K, Wang CL, Wang PX (2008) The effect of MMT/modified MMT on the structure and performance of the superabsorbent composite. *Polym Bull* 1:69–78
16. Paul MA, Alexandre M, Degee P, Henrist C, Rulmont A, Dubois P (2003) New nanocomposite materials based on plasticized poly (L-lactide) and organo-modified montmorillonites: thermal and morphological study. *Polymer* 2:443–450
17. Leu YY, Mohd Ishak ZA, Chow WS (2012) Mechanical, thermal, and morphological properties of injection molded poly (lactic acid)/SEBS-g-MAH/organo-montmorillonite nanocomposites. *J Appl Polym Sci* 2:1200–1207
18. Lee JW, Lim YT, Park OO (2000) Thermal characteristics of organoclay and their effects upon the formation of polypropylene/organoclay nanocomposites. *Polym Bull* 2:191–198
19. Katti KS, Sikdar D, Katti DR, Ghosh P, Verna D (2006) Molecular interactions in intercalated organically modified clay and clay-polycaprolactam nanocomposites: experiments and modeling. *Polymer* 1:403–414
20. Hayes MHB, Clapp CE (2001) Humic substances: considerations of compositions, aspects of structure, and environmental influences. *Soil Sci* 11:723–737
21. MacCarthy P (2001) The principles of humic substances. *Soil Sci* 11:738–751
22. Stevenson IL, Schnitzer M (1982) Transmission electron microscopy of extracted fulvic and humic acids 1. *Soil Sci* 3:179–185
23. Gondar D, Lopez R, Fiol S, Antelo JM, Arce F (2005) Characterization and acid–base properties of fulvic and humic acids isolated from two horizons of an ombrotrophic peat bog. *Geoderma* 3:367–374
24. Sierra MMD, Giovanela M, Parlanti E, SorianoSierra EJ (2005) Fluorescence fingerprint of fulvic and humic acids from varied origins as viewed by single-scan and excitation/emission matrix techniques. *Chemosphere* 6:715–733
25. Islam KMS, Schuhmacher A, Gropp JM (2005) Humic acid substances in animal agriculture. *Pakistan J Nutr* 3:126–134
26. Trckova M, Matlova L, Hudcova H, Faldyna M, Zraly Z, Dvorska L, Beran V, Pavlik I (2005) Peat as a feed supplement for animals: a review. *Vet Med* 50:361–377
27. Van Rensburg CEJ, Malfeld SCK, Dekker J (2001) Topical application of oxifulvic acid suppresses the cutaneous immune response in mice. *Drug Develop Res* 1:29–32
28. Lagaly G, Dekany I (2005) Adsorption on hydrophobized surfaces: clusters and self-organization. *Adv Colloid Interface Sci* 114–115:189–204
29. Brown JM, Curliss D, Vaia RA (2000) Thermoset-layered silicate nanocomposites. Quaternary ammonium montmorillonite with primary diamine cured epoxies. *Chem Mater* 12:3376–3384
30. Li Y, Ishida H (2003) Concentration-dependent conformation of alkyl tail in the nanoconfined space: hexadecylamine in the silicate galleries. *Langmuir* 6:2479–2484
31. Tsou CH, Suen MC, Yao WH, Yeh JT, Wu CS, Tsou CY, Chiu SH, Chen JC, Wang RY, Lin SM, Hung WS, Guzman MD, Hu CC, Lee KR (2014) Preparation and characterization of bioplastic-based green renewable composites from tapioca with acetyl tributyl citrate as a plasticizer. *Materials* 8:5617–5632
32. Jia QM, Zheng M, Chen HX, Shen RJ (2005) Synthesis and characterization of polyurethane/epoxy interpenetrating network nanocomposites with organoclays. *Polym Bull* 1–2:65–73

33. LeBaron PC, Wang Z, Pinnavaia TJ (1999) Polymer-layered silicate nanocomposites: an overview. *J Appl Clay Sci* 15:11–29
34. Mathew AP, Oksman K, Sain M (2005) Mechanical properties of biodegradable composites from poly lactic acid (PLA) and microcrystalline cellulose (MCC). *J Appl Polym Sci* 97:2014–2025
35. Aslzadeh MM, Abdouss M, Sadeghi GMM (2013) Preparation and characterization of new flame retardant polyurethane composite and nanocomposite. *J Appl Polym Sci* 3:1683–1690
36. Barick AK, Tripathy DK (2010) Preparation and characterization of thermoplastic polyurethane/organoclay nanocomposites by melt intercalation technique: effect of nanoclay on morphology, mechanical, thermal, and rheological properties. *J Appl Polym Sci* 2:639–654
37. Cheng S, Lau K, Liu T, Zhao YQ, Lam PM, Yin YS (2009) Mechanical and thermal properties of chicken feather fiber/PLA green composites. *Composites Part B: Eng* 40:650–654
38. Chow WS, Lok SK (2009) Thermal properties of poly (lactic acid)/organo-montmorillonite nanocomposites. *J Therm Anal Calorim* 95:627–632
39. Song P, Chen GY, Wei ZY, Zhang WX, Liang JC (2012) Rapid crystallization of poly (L-lactic acid) induced by a nanoscaled zinc citrate complex as nucleating agent. *Polymer* 19:4300–4309
40. Lopez RG, Trevino ME, Salazar LV, Peralta RD, Becerra F, Puig JE, Mendizabal E (1997) Polymerization of vinyl acetate in ternary microemulsions stabilized with hexadecyltrimethylammonium bromide. *Polym Bull* 4:411–417
41. Sathe SN, Devi S, Srinivasa Rao GS, Rao KV (1996) Relationship between morphology and mechanical properties of binary and compatibilized ternary blends of polypropylene and nylon 6. *J Appl Polym Sci* 61:97–107
42. Sathe SN, Srinivasa Rao GS, Rao KV, Devi S (1996) The effect of composition on morphological, thermal, and mechanical properties of polypropylene/nylon-6/polypropylene-g-butyl acrylate blends. *J Eng Sci* 36:2443–2450
43. Li B, Dong FX, Wang XL, Yang J, Wang DY, Wang YZ (2009) Organically modified rectorite toughened poly (lactic acid): nanostructures, crystallization and mechanical properties. *Euro Polym J* 11:2996–3003
44. Chow WS, Neoh SS (2009) Mechanical, morphological and thermal properties of polycarbonate/SEBS-G-MA/montmorillonite nanocomposites. *Polym-Plast Technol Eng* 49:62–68
45. Ray SS, Yamada K, Okamoto M, Ueda K (2003) Control of biodegradability of polylactide via nanocomposite technology. *Macromol Mater Eng* 3:203–208
46. Pluta M, Jeszka JK, Boiteux G (2007) Polylactide/montmorillonite nanocomposites: structure, dielectric, viscoelastic and thermal properties. *Euro Polym J* 7:2819–2835
47. Iannace S, Sabatini G, Ambrosio L, Nicolais L (1995) Mechanical behavior of composite artificial tendons and ligaments. *Biomaterials* 9:675–680
48. Ray SS, Okamoto M (2003) Biodegradable polylactide and its nanocomposites: opening a new dimension for plastics and composites. *Macromol Rapid Commun* 14:815–840
49. Lertwimolnun W, Vergnes B (2005) Influence of compatibilizer and processing conditions on the dispersion of nanoclay in a polypropylene matrix. *Polymer* 10:3462–3471